Immune landscape and TAM density in endometrial cancer: implications for immune checkpoint inhibitors efficacy

Olivia Le Saux (olivia.lesaux@lyon.unicancer.fr)
Renaud Sabatier
Isabelle Treilleux
Léa-Isabelle Renaud
Pierre-Emmanuel Brachet
Alejandra Martinez
Jean-Sébastien Frénel
Cyril Abdeddaim
Justine Berthet
Sarah Barrin
Amélie Colombe-Vermorel
Laetitia Odeyer
Alexandra Lainé
Christophe Caux
Bertrand Dubois
Isabelle Ray-Coquard

Research Article

Keywords: immune checkpoint inhibitors, macrophages, endometrial cancer

Posted Date: January 10th, 2024

DOI: https://doi.org/10.21203/rs.3.rs-3849068/v1

Additional Declarations: The authors declare potential competing interests as follows:

Abstract

Background

Although immune checkpoint inhibitors (ICI) have demonstrated their efficacy in endometrial cancer (EC), mismatch repair deficient/microsatellite instability high (MMRd/MSI-H) and mismatch repair proficient/microsatellite stable (MMRp/MSS) tumors present different sensitivity profiles to ICI. Moreover, a third of patients with MMRd/MSI-H tumors present primary resistance to ICI alone. We aimed to characterize dissimilarities in the tumor immune microenvironment of ICI-treated MMRd/MSI-H *vs* MMRp/MSS EC, and to identify possible mechanisms of resistance.

Methods

EC patients treated with ICI in 6 French comprehensive cancer centers were identified and classified as ICI-Responders or Non-Responders based on best objective response. A seven-color multi-immunofluorescence staining (CD20, CD4, CD8, FoxP3, CD68, CK, DAPI) was performed on sections from archival formalin-fixed paraffin-embedded primary tumors. Cell densities and spatial proximity were analyzed using inForm software. T/B lymphoid aggregates (LA) and Tertiary Lymphoid Structures (TLS) were separately quantified. Microsatellite status, presence of LA/TLS and immune cell densities were correlated to response to treatment.

Results

Twenty-one MMRd/MSI-H and 12 MMRp/MSS tumors were analyzed. We observed more MMRd/MSI-H tumors with LA/TLS compared to MMRp/MSS cases: 81% *vs* 17%, p = < 0.001. There were more CD8 + T effector cells in the vicinity of B cells in MMRd/MSI-H tumors compared to MMRp/MSS tumors (1.26 [0-3.40] *vs* 0.49 [0-1.86], *p* = 0.017), suggesting cooperation between effector T cells and B cells in MMRd/MSI-H tumors. No differences were shown in terms of the presence of LA/TLS and the subsequent response to ICI in EC (*p* = 0.400). Using a multivariate logistic regression model, we found that a low density of $CD68^+$ tumor-associated macrophages (TAMs) in the stroma, was associated with response to ICI in EC (Odds Ratio (OR) = 11.67, CI95 [1.69-237.45], p = 0.033) and showed good accuracy in predicting response to ICI in the whole cohort (AUC = 0.75, 95% CI [0.59–0.91]).

Conclusions

We provide a comprehensive characterization of the immune landscape in EC patients treated with ICIs. The distinct immune infiltrate patterns observed in MMRd/MSI-H and MMRp/MSS tumors, coupled with the significant negative association between TAM density and ICI response, underscore the potential of immune components as predictive biomarkers.

Introduction

Endometrial carcinoma (EC) is the most common gynecological cancer in western countries (1). While most patients with a localized disease have an excellent prognosis, a subset of patients presents recurrent and/or metastatic disease without treatment of curative intent. While carboplatin and paclitaxel have traditionally served as the established first-line therapy for advanced and recurrent EC, trials investigating the addition of immune checkpoint inhibitors (ICIs) have been successful. In four randomized trials, the ICIs dostarlimab, durvalumab, atezolizumab and pembrolizumab improved progression-free survival (PFS) when added individually to carboplatin and paclitaxel; with a trend for overall survival (OS) benefit in all-comers for some ICIs (2–5). Greatest PFS benefits were observed in those trials among those with mismatch repair deficiency (MMRd) (2, 3). Although the importance of the use of ICIs in EC is now established, some questions remain. Identification of the best combination in MMR proficient (MMRp)/microsatellite stable (MSS) tumors (chemotherapy, and/or anti-angiogenic therapy, and/or alternative therapies) still needs to be identified (5). Despite their ICIs-sensitive profile, 29–36.1% of MMRd/microsatellite instability high (MSI-H) will progress under ICI alone as reported in the Garnet and Keynote-158 trials (6, 7) and may require combination therapies. MMRd/MSI-H subtypes are characterized by a high tumor mutation burden (TMB) (8), increased infiltration by both T cells and B cells and higher expression of both PD-1 and PD-L1 (9), which could explain a better clinical response when treated with anti-PD-1/PD-L1 compared to MMRp/MSS patients. Indeed, tumor infiltrating B and T cells can organize into tertiary lymphoid structures (TLS) in EC (10) and these structures have been shown to be associated with response to ICIs in other solid tumors (11–13). In contrast, $CD68^+$ tumor associated macrophages (TAMs) and $CD4^+$ regulatory T cells (Tregs), which were found to be associated with EC aggressivity (14–17), could contribute to the limited efficacy of ICI in some patients (18–20). Herein, our objectives were firstly to characterize pre-treatment EC samples, followed by analyses of dissimilarities in the tumor immune micro-environment (TIME) of ICI-treated MMRd/MSI-H *vs* MMRp/MSS EC, and finally to identify possible mechanisms of resistance in EC, using *in situ* multispectral immunofluorescence tumor tissue staining and digital image analysis.

Methods

Patient cohort and tumor samples

EC patients treated with ICIs were identified by treating physicians from ARCAGY-GINECO (National Investigators Group for Ovarian and Breast Cancer Studies in France). Eligible patients were 18 years of age or older and had received immunotherapy (anti-PD-1, anti-PD-L1, anti-CTLA-4, or others) alone or in combination for a histologically confirmed advanced endometrial cancer. Patients with no primary tumor samples available or lost to follow-up were excluded. Archival formalin fixed paraffin embedded (FFPE) primary tumor samples were collected prospectively. All the available clinicopathologic information was retrieved from the clinical records for patients included. This included age, histology, initial FIGO stage, number of previous lines, MMRd/MSI-H status, p53 status, follow-up information for recurrence and vital

status. As per standard clinical practice, MMRd/MSI-H status was determined in priority in the basis of immunohistochemistry (IHC). In case of ambiguous result of IHC (lack of positive internal control, heterogeneous loss of MMR protein expression), the MMRd/MSI-H status was assessed by PCR/NGS. Patients were classified as ICI-Responders (R) (complete or partial response as best objective response-BOR) or Non-Responders (NR) (stable or progressive disease as BOR) according to local assessment.

Seven-colors multiplex immunofluorescence tissue staining

A hematoxylin and Eosin (H&E) stained slide of each sample was examined by a trained pathologist to confirm tissue quality, select samples for multi-IF staining and to annotate the tumor area. Seven-colors sequential multi-IF staining were performed with the BOND RX stainer (Leica Microsystems, Buffalo Grove, Illinois) using previously validated antibody (Ab) panels and a tonsil section was included in each staining batch to inspect the overall staining fidelity for all markers. After deparaffinization, rehydration and antigen retrieval, 4µm FFPE tumor sections were sequentially stained with each primary antibody, followed by OPAL-HRP secondary antibody incubation, and then revealed with tyramide signal amplification and OPAL fluorophores (Akoya Biosciences) and the same cycle was reproduced until staining with the last Ab of the panel. Slides were counter-stained with spectral DAPI (Akoya Biosciences) and cover slips were mounted using Prolong Gold medium (Invitrogen, Paisley, UK). Whole slides were imaged at a 20x magnification using the Vectra Polaris multispectral scanner (Akoya Biosciences).

Analysis of multi-IF digital images

Digital images were visualized with the Phenochart viewer (Akoya Biosciences) and representative regions of interests (ROI) (median 10, range [3–35] depending on the tumor surface) were selected by OLS. After spectral unmixing using the synthetic library of the inForm software (Akoya Biosciences), tissue and cell segmentation was performed as for the other multi-IF panel to classify tumor, followed by cell phenotyping. A machine learning algorithm was trained by user-specified tissue annotations aided by the signal from the epithelial marker to accurately segment tumor tissue versus stromal tissue and background, as well as individual cells using the nuclear DAPI signal. The algorithm was trained (1/3) and validated (2/3) on 1 to 2 ROI selected from each tumor samples to be representative of the cohort before launching the batch analysis on all slides. After manual inspection, the algorithm was again optimized, if necessary, until correct segmentation and phenotyping (> 80% of cells correctly identified). Different phenotypes were analyzed: $CD20^+$ as B cells, $CD68^+$ as TAMs, $CD4^+/CD68^-/FOXP3^-$ as CD4 helper T cells, $CD4^+/CD68^-/FOXP3^+$ as CD4 regulatory T cells, CD8+/$FOXP3^-$ as CD8 effector T cells and $CD8^+/FOXP3^+$ T cells. Finally, the phenotyping data were exported from inForm and tabulated reports including cell densities, and spatial analyses (count within radius – 20µm) were obtained using the R package phenoptr or PhenoptrReports (Akoya Biosciences). TLS were defined as dense aggregates of $CD20^+$ cells (B-follicle) adjacent to T cell ($CD4^+$) rich areas on whole slides. Lymphoid aggregates were vague, ill-defined clusters of lymphocytes without a clear separate B-follicle and T-cell zone.

Statistical analysis

Statistical analyses were performed using R programming language (v4.0.2). Non-parametric statistical tests were used. Survival analysis included Kaplan-Meier estimators, and likelihood ratio (LR) tests due to small sample size. Duration of response was defined as the time from onset of response to progression or death due to any reason, whichever occurs earlier. Tests *P*-values < 0.05 were statistically significant. No statistical comparison was performed to compare response rate and survival between MMRd/MSI-H and MMRp/MSS tumors due to the heterogeneity in therapies received. The initial phase involved a comparison of immune cell density and presence of LA/TLS between MMRd/MSI-H and MMRp/MSS tumors. In the second phase, immune cell density and presence of LA/TLS were compared between R and NR in the whole cohort. Multivariate logistic regression models were generated using logistic regression with least absolute shrinkage and selection operator (LASSO) penalty for response to therapy. This model allows both variables selection and regression coefficients estimation by maximizing the log-likelihood function. This model is used in cases of several potential markers to test in the model relatively to the number of observations. LASSO regression analysis was applied to microsatellite status, presence of lymphoid aggregate and TLS, and density of immune cells with p-values < 0.05, as estimated through univariable Wilcoxon tests. Tenfold cross-validation was utilized to determine the optimal value of penalty parameter λ within 1 standard deviation from the minimum (λ = 0.15).

Ethics approval

The study was registered on September 4th, 2020, by the Data Protection Officer of the Centre Léon Bérard on the activity registry of the institution (Ref. R201-004-086). This study falls within the scope of the French Reference Methodology MR-004 according to 2016–41 law dated 26 January 2016. This study was conducted according to the REMARK (recommendations for tumor marker prognostic studies) criteria (21).

Results

Patients' characteristics

A total of 33 advanced endometrial cancer (EC) patients pre-treated with ICIs from 2016 to 2021 in six French Cancer Centers were included. Patients' characteristics are described in Table 1. Mean age was 64 years ± standard deviation (SDev) 9.41. Patients with initial FIGO stages IV comprised more than 80% of the population. All patients with MMRd/MSI-H tumor and MLH-1 promotor methylation status assessment (data missing in 7 cases) displayed a hyper methylation profile suggesting a somatic origin of MMR deficiency. p53 immunohistochemistry status was not available in most MMRp/MSS tumors (10/12, 83%). Every patient received monoclonal antibodies targeting PD-1/PD-L1, most of them as monotherapy (58%). Most patients whose tumors were MMRd/MSI-H received anti-PD-1/PD-L1 antibodies monotherapy (67%) while half of patients with MMRp/MSS tumors received Pembrolizumab + Lenvatinib (50%) (Table 1). The best objective response rate (BOR) was 26%, 95%CI [13–46] *vs* 25%, 95%CI [9–53] in MMRd/MSI-H and MMRp/MSS groups, respectively. Median duration of response was 34.5 months (range: 8.0–57.0) and 18 months (range: 16.0–24.0) in MMRd/MSI-H and MMRp/MSS

groups, respectively (Fig. 1). Median follow-up was 16 months 95%CI [7–21]. Median progression-free survival (PFS) was 3.5, 95% CI [3-not reached, NR] *vs* 6.5 months 95%CI [2.0-NR] in the MMRd/MSI-H and MMRp/MSS group, respectively, with, as expected, a tail of curve PFS benefit in the MMRd/MSI-H group (**Supp** Fig. 1A). Median OS was not reached in the MMRd/MSI-H group 95%CI [16.0-NR] and was of 7.5 months in the MMRp/MSS group 95% CI [5.0-NR] (**Supp** Fig. 1B).

Table 1

Clinical and demographic characteristics of the patients. Indicated FIGO stages are at the time of the initial diagnosis. When receiving ICI, all patients were in relapse setting (with met localisations). No Lynch syndrome was identified in this cohort of patients. *[1] One patient was treated with anti-PD1 + Netrin-1 inhibitor only (NCT04652076) and one patient with anti-PD1 + IDO inhibitor only (NCT03459222). *[2] One patient was treated with anti-PD1 followed by anti-PD-1 + anti-CTLA-4 after progression during PD1 inhitor therapy and another patient was treated with anti-PD1 + Netrin-1 inhibitor followed by anti-PD-1 + anti-CTLA-4 at progression. Other histological types include undifferentiated n = 1, carcinosarcoma n = 1, and clear cell n = 1. *MMRd, mismatch repair deficient; MMRp, mismatch repair proficient; MSI-H, microsatellite instability high; MSS, microsatellite stability; SDev, standard deviation; CT, chemotherapy; ET, endocrine therapy.*

Variables	Total (n = 33)	MMRd/MSI-H (n = 21)	MMRp/MSS (n = 12)	*P*-value
Age, Mean ± SDev	63.55 ± 9.41	65.43 ± 9.42	60.25 ± 8.82	0.126
Histological type, n (%)				0.003
Endometrioid	28 (85)	21 (100)	7 (58)	
Mixed	1 (3)	0 (0)	1 (8)	
Other	3 (9)	0 (0)	3 (25)	
Serous	1 (3)	0 (0)	1 (8)	
FIGO stage, n (%)				0.328
IIIC	5 (15)	2 (10)	3 (25)	
IV	28 (85)	19 (90)	9 (75)	
Protein loss, n (%)				NA
MLH1/PMS2	18 (55)	18 (86)	0 (NaN)	
MSH2/MSH6	2 (6)	2 (10)	0 (NaN)	
NaN	13 (39)	1 (4)	0 (NaN)	
MLH1 promoter hypermethylation, n (%)	14 (42)	14 (67)	0 (NaN)	NA
NaN	19 (58)	7 (33)	0 (NaN)	
Therapy received, n (%)				0.004
Anti-PD1/PDL1 alone	19 (54)	14 (61)	5 (42)	
+ Anti-CTLA-4	6 (17)	6 (26)	0 (0)	
+ Lenvatinib	7 (20)	1 (4)	6 (50)	
+ Other (NP137, IDO inhibitor)*1	3 (9)	2 (9)	1 (8)	

Variables	Total (n = 33)	MMRd/MSI-H (n = 21)	MMRp/MSS (n = 12)	*P*-value
Number of previous lines including ET, n (%)*2				0.658
1	19 (54)	14 (61)	5 (42)	
2	10 (29)	5 (22)	5 (42)	
≥3	6 (17)	4 (17)	2 (17)	
Number of previous CT lines, n (%)*2				> 0.99
1	25 (71)	16 (70)	9 (75)	
2	7 (20)	5 (22)	2 (17)	
≥3	3 (9)	2 (10)	1 (8)	

EC tumor immune infiltrate characteristics

By using a 7-colors multiplexed-immunofluorescence (multi-IF) staining (CD20, CD4, CD8, FoxP3, CD68, panCK, DAPI), we characterized, for each tumor sample collected at tumor diagnosis, the presence of lymphoid aggregates (LA)/tertiary lymphoid structures (TLS) (Fig. 2A), and the density of $CD20^+$ B cells, CD4 + T helper cells (Th; $CD4^+FOXP3^-$), regulatory T cells (Tregs; $CD4^+FOXP3^+$), CD8 + T effector cells (Teffs; $CD8^+FOXP3^-$), $CD8^+FOXP3^+$ T cells, and $CD68^+$ tumor-associated macrophages (TAMs) both in the stroma and the tumor islets (Fig. 2B). Tumor samples used were primary tumor samples collected at diagnosis so not at the time of ICI initiation. The majority of patients had received one previous line of therapy (54%, Table 1) between tumor sampling and ICI initiation. Immune cells were mostly located in the stroma of EC with a majority of $CD4^+$ Th cells (mean: 654 cells/mm^2 ± SDev 429) and tumor-associated macrophages (TAMs) (620 cells/mm^2 ± SDev 452) followed by $CD8^+$ Teffs cells (383 cells/mm^2 ± SDev 326) (Fig. 2B). Within tumor islets, $CD8^+$ Teffs cells were the most prevalent immune cell subtype (94 cells/mm^2 ± SDev 136) (Fig. 2B). B cells and Tregs were scarce within tumors, but their occurrence was higher in the stroma and variable based on individual patients (Fig. 2B).

LA/TLS are present in the vast majority of MMRd/MSI-H tumors.

In response to the differing efficacy of ICI in EC molecular subtypes, we investigated the tumor immune profile based on EC genomic status. MMRd/MSI-H tumors displayed higher densities of both B cells and $CD4^+$ Th cells in the stroma compared to MMRp/MSS tumors (236 cells/mm^2 ± SDev 374 *vs* 166 cells/mm^2 ± SDev 423, $p = 0.027$ for B cells, and 804 cells/mm^2 ± SDev 430 *vs* 391 cells/mm^2 ± SDev 284, $p = 0.007$ for CD4 + Th cells). (Fig. 3A). In line with the variations noted among B cells and CD4 + Th cells, which together form LA/TLS, we observed more MMRd/MSI-H tumors with LA/TLS compared to

MMRp/MSS cases: 81% *vs* 17% respectively, $p < 0.001$ (Fig. 3B). To gain a deeper insight into cell interactions involving LA/TLS and other cells, we examined the cellular environment within a 20 µm radius around B and CD4 + Th cells (**Supp** Table 1). There were more TAMs (1.23 ± SDev 0.95 *vs* 0.62 ± SDev 0.54, $p = 0.041$) and $CD8^+$ Teffs cells (1.45 ± SDev 1.05 *vs* 0.62 ± SDev 0.57, $p = 0.017$) in the vicinity of B cells in MMRd/MSI-H tumors compared to MMRp/MSS tumors respectively suggesting cooperation between TAM and B cells and between effector T cells and B cells in MMRd/MSI-H tumors (**Supp** Table 1). In summary, a higher presence of LA/TLS and increased proximity between B and effector T cells are observed in MMRd/MSI-H EC, potentially elucidating a higher sensitivity to immune checkpoint inhibitors (ICI) (11–13).

Resistance to immune checkpoint inhibitors is associated with a significant abundance of TAMs in the stroma in EC.

We then categorized patients according to their response to treatment. Eight responder (R) patients (25%) were compared to 24 non-responder patients (NR) (75%). R patients' tumors had less TAMs (357 cells/mm^2 ± SDev 117 *vs.* 706 cells/mm^2 ± SDev 498 in the stroma, $p = 0.043$; and 15 cells/mm^2 ± SDev 31 *vs* 28 cells/mm^2 ± SDev 33 in tumor islets, $p = 0.028$) and less $CD4^+$ Th cells in tumor islets (13 cells/mm^2 ± SDev 17 *vs.* 30 cells/mm^2 ± SDev 40, $p = 0.037$) (Fig. 4A). No differences were shown in terms of the presence of LA/TLS and the subsequent response ($p = 0.400$) (Fig. 4B). To identify significant and independent biomarkers associated with response, we used a multivariate logistic regression model featuring least absolute shrinkage and selection operator (LASSO). This model encompassed all density biomarkers correlated significantly with ICI response in univariate analysis, alongside the presence of LA/TLS (a recognized predictive biomarker) and microsatellite status. We found that the density of TAM in the stroma was the only independent predictive factor associated with response. A low density of TAM in the stroma, below the median, was associated with response (Odds Ratio (OR) = 11.67, CI95 [1.69-237.45], $p = 0.033$. A low density of TAMs in the stroma showed good accuracy in predicting response to ICI in the whole cohort (AUC = 0.75, 95% CI = 0.59–0.91) but also in MMRd/MSI-H tumors (AUC = 0.70, 95% CI = 0.47–0.93) and in MMRp/MSS tumors (AUC = 0.83, 95% CI = 0.67–0.99) (Fig. 4C). A low proportion of TAMs in the stroma did not show an association with progression-free survival (PFS, HR = 0.59 [0.25–1.38], $p = 0.2$) but exhibited a significant correlation with overall survival (OS, HR = 0.27 [0.10–0.77], $p = 0.009$ LR test) (Fig. 4D). As an illustration, Fig. 4E shows one NR EC patient with a high number of TAMs the stroma and a R patient with few TAMs in the stroma (Fig. 4E).

Discussion

The landscape of immune cell infiltration within the tumor microenvironment (TME) has emerged as a crucial determinant of response to ICIs in various cancer types (22). In this study, we investigated the immune characteristics of EC patients treated with ICIs, using *in situ* multispectral immunofluorescence tumor tissue staining and digital image analysis, aiming to unravel the intricate relationship between tumor immune infiltrate, LA/TLS, and TAMs in influencing ICI response.

Our investigation into the immune profile based on genomic status highlighted significant differences between MMRd/MSI-H and MMRp/MSS tumors. MMRd/MSI-H tumors exhibited elevated densities of B cells and CD4 + T helper cells within the stromal compartment, corroborating previous studies indicating a more inflamed microenvironment in MSI-H tumors as expected due to a higher number predicted neoantigens (23, 24). Moreover, the increased prevalence of LA/TLS in MMRd/MSI-H tumors underscores their potential role in facilitating immune cell interactions and immune priming of T cells with anti-tumor activity (25). This corroborates the increased proximity between B and effector T cells observed in MMRd/MSI-H compared to MMRp/MSS EC. Those observations align with emerging evidence linking LA/TLS with favorable ICI responses, indicating a potential biomarker for therapeutic efficacy in EC (11–13). On the other hand, we do not report any significant differences in terms of effector T cells density. Differences in infiltrating immune cells, with higher $CD8^+$ immune cells and lower $CD68^+$ TAMs, have been noted between Lynch syndrome (LS)-associated compared with sporadic MMRd/MSI-H EC (24, 26). This could be explained by the fact that no LS-associated MMRd/MSI-H tumors were included in this cohort.

The frequency of patients harboring TLS is rather low, ranging from 19% in the PORTEC trial in localized 1st line therapy compared to a quarter of cases for structured lymphoid aggregates in cohorts including patients whose disease had progressed (10). Tumor infiltration by TAMs, identified by the expression of CD68, was similar in both molecular subgroups but was lower in R compared to NR, implicating TAMs in mediating immune resistance. This finding is in line with recent studies that have highlighted the role of TAMs in fostering an immunosuppressive microenvironment, thereby limiting the efficacy of ICIs (27, 28). The accuracy of TAM density in predicting ICI response in both MMRd/MSI-H and MMRp/MSS tumors underscores its potential as a universal predictive biomarker. Interestingly, MMRd/MSI-H tumors displayed a higher proportion of TAMs in the vicinity of B cells compared to MMRp/MSS tumors potentially explaining the low response rate reported in our MMRd/MSI-H cohort compared to the literature. While TAMs have been recognized as crucial for the development of high endothelial venules and TLS formation (29), some studies indicate a potential inhibitory effect on B cell proliferation (30) and a downregulation of germinal center reaction (31). This might provide insight into the adverse impact of a high macrophage density within TLS on cancer patients' survival (32). Additionally, it is noteworthy that these TAMs could display characteristics similar to the M2-like phenotype. We can then hypothesize that targeting TAMs in patients in combination with conventional ICIs might increase survival.

Despite the insights gained, our study has limitations. The small sample size and retrospective nature of the analysis warrant cautious interpretation of the results. Due to sample size issues, we were unable to perform subgroup analyses to identify the respective impact of the immune parameters according to the type of therapy received. Additionally, the lack of availability of p53 immunohistochemistry status in a subset of tumors could introduce confounding variables. p53 IHC status was not available in most of the cases mainly because the sample collection was performed before the implementation of molecular classification in routine. Additionally, the specimens of tumors utilized for examination were procured at the time of tumor diagnosis and exclusively comprised tissues from the endometrial site. Despite patients

undergoing at least one treatment regimen between the collection of tumor samples and ICI initiation, we assert that focusing solely on endometrial samples helped mitigate potential bias associated with variations in immune composition across different anatomical sites (such as the liver, endometrium, lymph nodes, etc.). Future studies with larger cohorts and prospective designs are needed to validate our findings and explore the underlying mechanisms driving the observed associations.

In summary, our study provides a comprehensive characterization of the immune landscape in EC patients treated with ICIs. The distinct immune infiltrate patterns observed in MMRd/MSI-H and MMRp/MSS tumors, coupled with the significant association between TAM density and ICI response, underscore the potential of immune components as predictive biomarkers. The intricate links between TAMs, immune cell subtypes, and LA/TLS within the TME offers valuable insights into the determinants of ICI sensitivity and resistance. Further exploration of TAM-targeted strategies may hold the key to enhancing ICI efficacy and improving outcomes in EC patients. However, the clinical implementation of TAM-targeting strategies aiming at depleting or repolarizing TAMs has been limited to date, mostly due to the high heterogeneity and plasticity of TAMs (33). Enhancing our understanding of TAM biology, differentiating markers, and interactions with immune and non-immune cells is essential for developing successful anticancer treatments.

List Of Abbreviations

BOR best objective response

CR complete response

CT chemotherapy

CTLA-4 Cytotoxic T-Lymphocyte-Associated protein-4

EC endometrial cancer

ET endocrine therapy

FFPE formalin fixed paraffin embedded

FIGO Fédération internationale de gynécologie et d'obstétrique

H&E hematoxylin&eosin

ICI immune checkpoint inhibitor

IDO Indoleamine 2, 3-dioxygenase

IF immunofluorescence

IHC immunohistochemistry

LA lymphoid aggregate

LASSO least absolute shrinkage and selection operator

MMRd mismatch repair deficient

MMRp mismatch repair proficient

MSI-H microsatellite instability-high

MSS microsatellite stable

NCT national clinical trials

NR non-responder

OS overall survival

PD progressive disease

PD-1 Programmed death 1

PD-L1 Programmed death-ligand 1

PFS progression-free survival

PR partial response

R responder

SD stable disease

SDev standard deviation

TAM tumor-associated macrophage

Teff effector T cell

Th T helper cell

TLS tertiary lymphoid structure

TME tumor micro-environment

Treg regulatory T cell

Declarations

Ethics approval and consent to participate

The study was registered on September 4th, 2020, by the Data Protection Officer of the Centre Léon Bérard on the activity registry of the institution (Ref. R201-004-086). This study falls within the scope of the French Reference Methodology MR-004 according to 2016–41 law dated 26 January 2016. This study was conducted according to the REMARK (recommendations for tumor marker prognostic studies) criteria (21).

Consent for publication

Not applicable

Availability of data and material

Not applicable

Competing interests

AM received honoraria from GSK. JSF received honoraria from Astrazeneca, Daïchi, Pfizer, Lilly, Novartis, Gsk, MSD, Esai, Seagen. IRC received research grants from MSD, Roche, BMS, GSK, Novartis, Astra Zeneca and Merck Sereno; honoraria from Abbvie, Agenus, Advaxis, BMS, PharmaMar, Genmab, Pfizer, AstraZeneca, Roche/Genentech, GSK, MSD, Deciphera, Mersena, Merck Sereno, Novartis, Amgen, Tesaro and Clovis; Springworks, Adaptimmune, Immunogen, Seagen, Novocure, Daichi Sankyo; and travel support from support from Roche, AstraZeneca and GSK. RS received research grants from Astra-Zeneca, honoraria from Astra-Zeneca, GSK, Seagen, EISAI, Novartis, Clovis Oncology, non-financial support from MSD, GSK, Novartis. OLS received research grants from Astrazeneca and honoraria from GSK, MSD and Clovis Oncology.

Funding

Rhône Alpes Auvergne region (Grant IRICE RRA18 010792 01 – 10365) for initial funding of the LICL multi-IF platform.

Authors' contributions

O.L.S, B.D., I.T. C.C and I.R.C designed the work. O.L.S, S.B., L.I.R, J.B, L.O, and A.C participated in the data acquisition, analysis. O.L.S, R.S., B.D, I.R.C, C.C, A.L., L.I.R, J.S.F., A.M., C.A., and P.E.B participated in the interpretation of data. All authors drafted the work or substantively revised it.

Acknowledgements

Not applicable.

References

1. Bray F, Ferlay J, Soerjomataram I, Siegel RL, Torre LA, Jemal A. Global cancer statistics 2018: GLOBOCAN estimates of incidence and mortality worldwide for 36 cancers in 185 countries. CA Cancer J Clin. 2018;68(6):394–424.
2. Mirza MR, Chase DM, Slomovitz BM, dePont Christensen R, Novák Z, Black D, et al. Dostarlimab for Primary Advanced or Recurrent Endometrial Cancer. N Engl J Med. 27 mars 2023;0(0):null.
3. Eskander RN, Sill MW, Beffa L, Moore RG, Hope JM, Musa FB, et al. Pembrolizumab plus Chemotherapy in Advanced Endometrial Cancer. N Engl J Med. 8 juin 2023;388(23):2159–70.
4. Colombo N, Harano K, Hudson E, Galli F, Antill Y, Choi CH, et al. LBA40 Phase III double-blind randomized placebo controlled trial of atezolizumab in combination with carboplatin and paclitaxel in women with advanced/recurrent endometrial carcinoma. Ann Oncol. 1 oct 2023;34:S1281–2.
5. Westin SN, Moore K, Chon HS, Lee JY, Pepin JT, Sundborg M, et al. Durvalumab Plus Carboplatin/Paclitaxel Followed by Maintenance Durvalumab With or Without Olaparib as First-Line Treatment for Advanced Endometrial Cancer: The Phase III DUO-E Trial. J Clin Oncol Off J Am Soc Clin Oncol. 21 oct 2023;101200JCO2302132.
6. Oaknin A, Gilbert L, Tinker AV, Brown J, Mathews C, Press J, et al. Safety and antitumor activity of dostarlimab in patients with advanced or recurrent DNA mismatch repair deficient/microsatellite instability-high (dMMR/MSI-H) or proficient/stable (MMRp/MSS) endometrial cancer: interim results from GARNET-a phase I, single-arm study. J Immunother Cancer. janv 2022;10(1):e003777.
7. O'Malley DM, Bariani GM, Cassier PA, Marabelle A, Hansen AR, De Jesus Acosta A, et al. Pembrolizumab in Patients With Microsatellite Instability-High Advanced Endometrial Cancer: Results From the KEYNOTE-158 Study. J Clin Oncol Off J Am Soc Clin Oncol. 1 mars 2022;40(7):752–61.
8. Chalmers ZR, Connelly CF, Fabrizio D, Gay L, Ali SM, Ennis R, et al. Analysis of 100,000 human cancer genomes reveals the landscape of tumor mutational burden. Genome Med. 19 avr 2017;9:34.
9. Talhouk A, Derocher H, Schmidt P, Leung S, Milne K, Gilks CB, et al. Molecular Subtype Not Immune Response Drives Outcomes in Endometrial Carcinoma. Clin Cancer Res. 15 avr 2019;25(8):2537–48.
10. Horeweg N, Workel HH, Loiero D, Church DN, Vermij L, Léon-Castillo A, et al. Tertiary lymphoid structures critical for prognosis in endometrial cancer patients. Nat Commun. 16 mars 2022;13(1):1373.
11. Petitprez F, de Reyniès A, Keung EZ, Chen TWW, Sun CM, Calderaro J, et al. B cells are associated with survival and immunotherapy response in sarcoma. Nature. 2020;577(7791):556–60.
12. Cabrita R, Lauss M, Sanna A, Donia M, Skaarup Larsen M, Mitra S, et al. Tertiary lymphoid structures improve immunotherapy and survival in melanoma. Nature. 2020;577(7791):561–5.
13. Helmink BA, Reddy SM, Gao J, Zhang S, Basar R, Thakur R, et al. B cells and tertiary lymphoid structures promote immunotherapy response. Nature. 2020;577(7791):549–55.
14. Kübler K, Ayub TH, Weber SK, Zivanovic O, Abramian A, Keyver-Paik MD, et al. Prognostic significance of tumor-associated macrophages in endometrial adenocarcinoma. Gynecol Oncol. nov 2014;135(2):176–83.

15. Dun EC, Hanley K, Wieser F, Bohman S, Yu J, Taylor RN. Infiltration of tumor-associated macrophages is increased in the epithelial and stromal compartments of endometrial carcinomas. Int J Gynecol Pathol Off J Int Soc Gynecol Pathol. nov 2013;32(6):576–84.
16. Yamagami W, Susumu N, Tanaka H, Hirasawa A, Banno K, Suzuki N, et al. Immunofluorescence-detected infiltration of CD4 + FOXP3 + regulatory T cells is relevant to the prognosis of patients with endometrial cancer. Int J Gynecol Cancer Off J Int Gynecol Cancer Soc. déc 2011;21(9):1628–34.
17. Makker V, MacKay H, Ray-Coquard I, Levine DA, Westin SN, Aoki D, et al. Endometrial cancer. Nat Rev Dis Primer. 9 déc 2021;7(1):88.
18. Peranzoni E, Lemoine J, Vimeux L, Feuillet V, Barrin S, Kantari-Mimoun C, et al. Macrophages impede CD8 T cells from reaching tumor cells and limit the efficacy of anti-PD-1 treatment. Proc Natl Acad Sci U S A. 24 avr 2018;115(17):E4041–50.
19. Kumagai S, Togashi Y, Kamada T, Sugiyama E, Nishinakamura H, Takeuchi Y, et al. The PD-1 expression balance between effector and regulatory T cells predicts the clinical efficacy of PD-1 blockade therapies. Nat Immunol. nov 2020;21(11):1346–58.
20. Gorvel L, Olive D. Tumor associated macrophage in HPV + tumors: Between immunosuppression and inflammation. Semin Immunol. janv 2023;65:101671.
21. McShane LM, Hayes DF. Publication of Tumor Marker Research Results: The Necessity for Complete and Transparent Reporting. J Clin Oncol. 1 déc 2012;30(34):4223–32.
22. Zhang Y, Zhang Z. The history and advances in cancer immunotherapy: understanding the characteristics of tumor-infiltrating immune cells and their therapeutic implications. Cell Mol Immunol. août 2020;17(8):807–21.
23. Suemori T, Susumu N, Iwata T, Banno K, Yamagami W, Hirasawa A, et al. Intratumoral CD8 + Lymphocyte Infiltration as a Prognostic Factor and Its Relationship With Cyclooxygenase 2 Expression and Microsatellite Instability in Endometrial Cancer. Int J Gynecol Cancer Off J Int Gynecol Cancer Soc. sept 2015;25(7):1165–72.
24. Pakish JB, Zhang Q, Chen Z, Liang H, Chisholm GB, Yuan Y, et al. Immune Microenvironment in Microsatellite-Instable Endometrial Cancers: Hereditary or Sporadic Origin Matters. Clin Cancer Res Off J Am Assoc Cancer Res. 1 août 2017;23(15):4473–81.
25. Teillaud JL, Dieu-Nosjean MC. Tertiary Lymphoid Structures: An Anti-tumor School for Adaptive Immune Cells and an Antibody Factory to Fight Cancer? Front Immunol. 21 juill 2017;8:830.
26. Ramchander NC, Ryan NAJ, Walker TDJ, Harries L, Bolton J, Bosse T, et al. Distinct Immunological Landscapes Characterize Inherited and Sporadic Mismatch Repair Deficient Endometrial Cancer. Front Immunol. 2019;10:3023.
27. Zhu Y, Knolhoff BL, Meyer MA, Nywening TM, West BL, Luo J, et al. CSF1/CSF1R Blockade Reprograms Tumor-Infiltrating Macrophages and Improves Response to T-cell Checkpoint Immunotherapy in Pancreatic Cancer Models. Cancer Res. 14 sept 2014;74(18):5057–69.
28. Georgoudaki AM, Prokopec KE, Boura VF, Hellqvist E, Sohn S, Östling J, et al. Reprogramming Tumor-Associated Macrophages by Antibody Targeting Inhibits Cancer Progression and Metastasis. Cell

Rep. 31 mai 2016;15(9):2000–11.

29. Johansson-Percival A, He B, Li ZJ, Kjellén A, Russell K, Li J, et al. De novo induction of intratumoral lymphoid structures and vessel normalization enhances immunotherapy in resistant tumors. Nat Immunol. nov 2017;18(11):1207–17.
30. Goldman N, Valiuskyte K, Londregan J, Swider A, Somerville J, Riggs JE. Macrophage regulation of B cell proliferation. Cell Immunol. avr 2017;314:54–62.
31. Smith JP, Burton GF, Tew JG, Szakal AK. Tingible body macrophages in regulation of germinal center reactions. Dev Immunol. 1998;6(3–4):285–94.
32. Yamaguchi K, Ito M, Ohmura H, Hanamura F, Nakano M, Tsuchihashi K, et al. Helper T cell-dominant tertiary lymphoid structures are associated with disease relapse of advanced colorectal cancer. Oncoimmunology. 2020;9(1):1724763.
33. Pittet MJ, Michielin O, Migliorini D. Clinical relevance of tumour-associated macrophages. Nat Rev Clin Oncol. juin 2022;19(6):402–21.

Figures

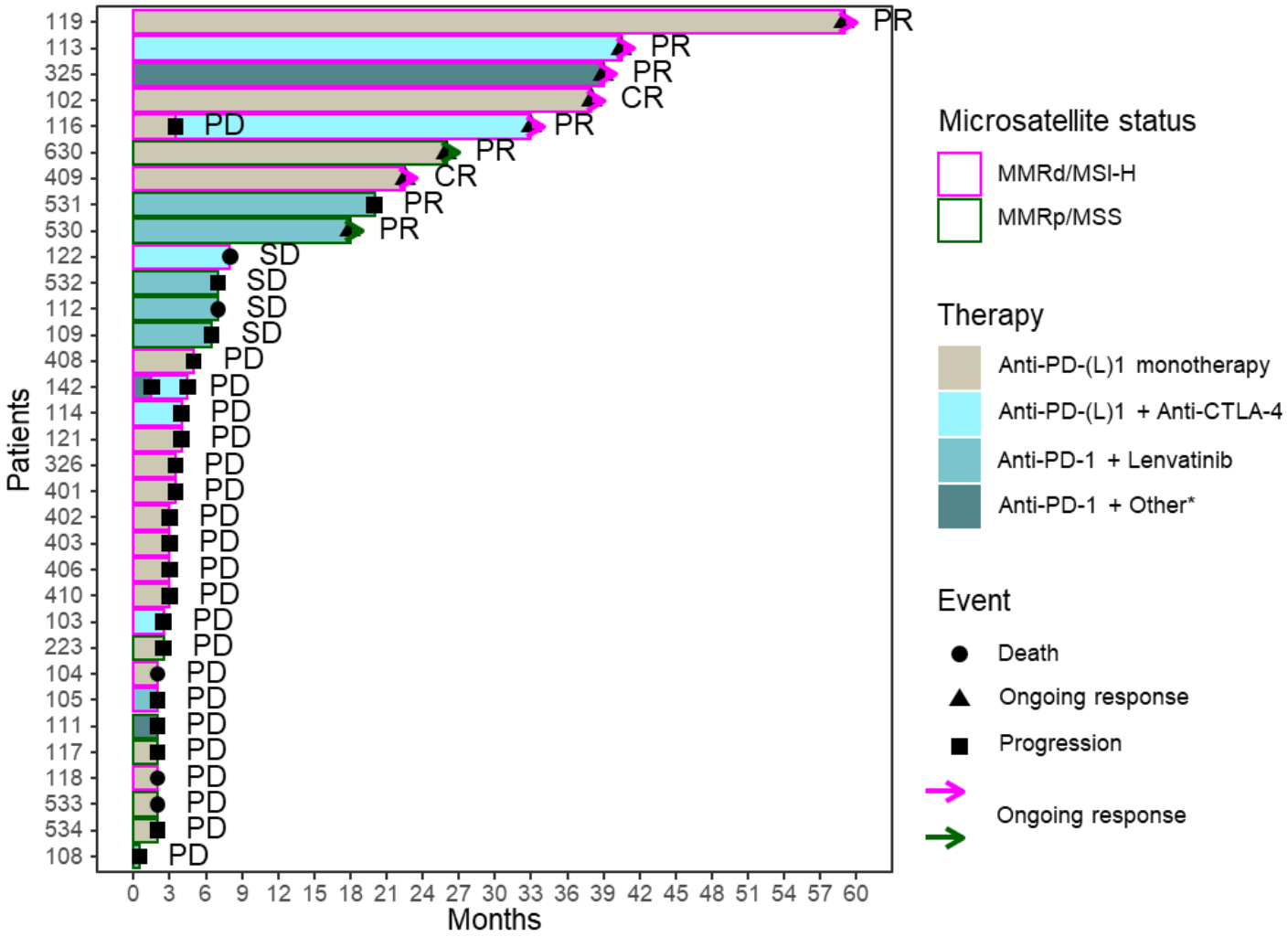

Figure 1

Swimmer plot of treatment and disease course. Each bar represents a patient. *142 and 111 were treated with anti-PD1 + Netrin-1 inhibitor (NCT04652076) and 326 with anti-PD1 + IDO inhibitor (NCT03459222). *Best objective response includes CR, complete response, PR, partial response, SD, stable disease, PD, progressive disease; MMRd, mismatch repair deficient; MMRp, mismatch repair proficient; MSI-H, microsatellite instability high; MSS, microsatellite stability.*

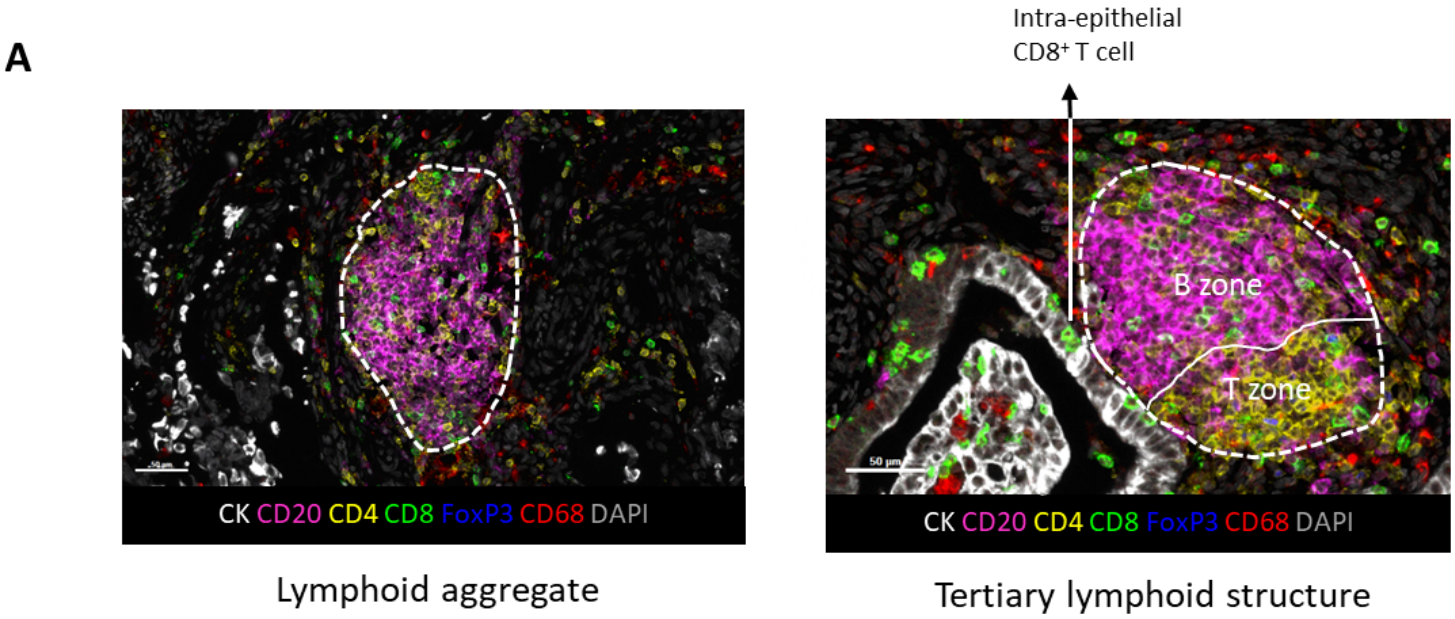

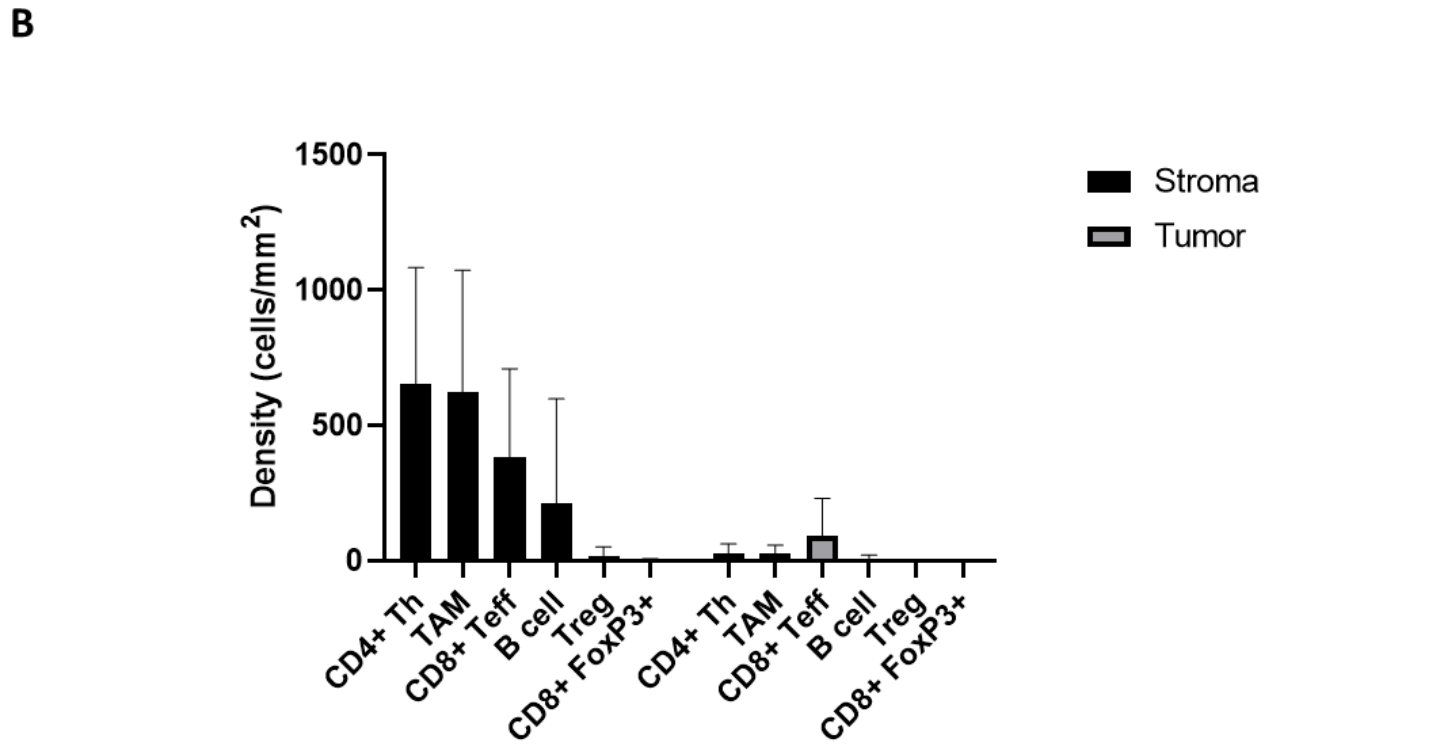

Figure 2

Density of immune cells in endometrial carcinoma in the tumor and the stroma.

A – Representative image of multi-IF staining showing a tumor sample with lymphoid aggregate (left) and another sample with a TLS and intra-epithelial CD8+ Teffs cells (in green) (right).

B – Number of cells/mm^2 (i.e., the density) of B cells, TAMs, CD4$^+$ T helper (Th) cells, CD4$^+$ regulatory T cells (Treg), CD8$^+$ effector T cells (Teff) and CD8$^+$/FOXP3$^+$ T cells both in the stroma (black) and the tumor (grey) in EC. Mean and standard deviations are displayed.

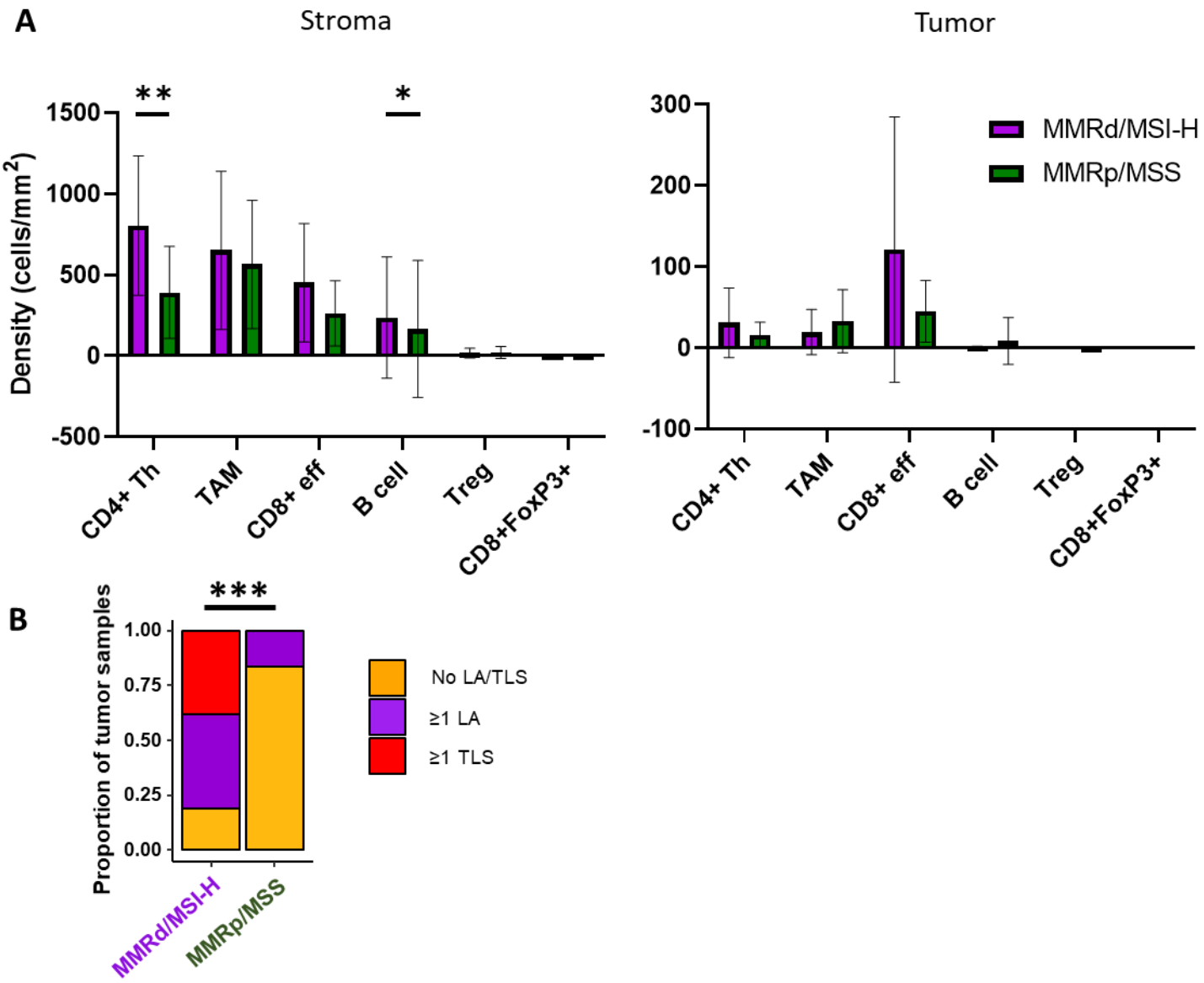

Figure 3

A greater percentage of MMRd/MSI-H tumors exhibit LA/TLS in comparison to MMRp/MSS tumors.

A – Number of cells/mm^2 (i.e., the density) of B cells, TAMs, CD4$^+$ T helper (Th) cells, CD4$^+$ regulatory T cells (Treg), CD8$^+$ effector T cells (Teff) and CD8$^+$/FOXP3$^+$ T cells both in the stroma (left) and within

tumor islets (right) in MMRd/MSI-H (magenta) and MMRp/MSS (dark green) tumors. Mean and standard deviations are displayed.

B – Proportion of MMRd/MSI-H (magenta) / MMRp/MSS (darkgreen) samples with (≥1 lymphoid aggregate -LA- in the sample or ≥1 tertiary lymphoid structure -TLS- in the sample) and without TLS (no TLS in the sample). *P*-values < 0.05 were considered significant, with stars corresponding to * $p < 0.05$; ** $p < 0.01$; *** $p < 0.001$. If no stars are indicated, no statistically significant difference was found.

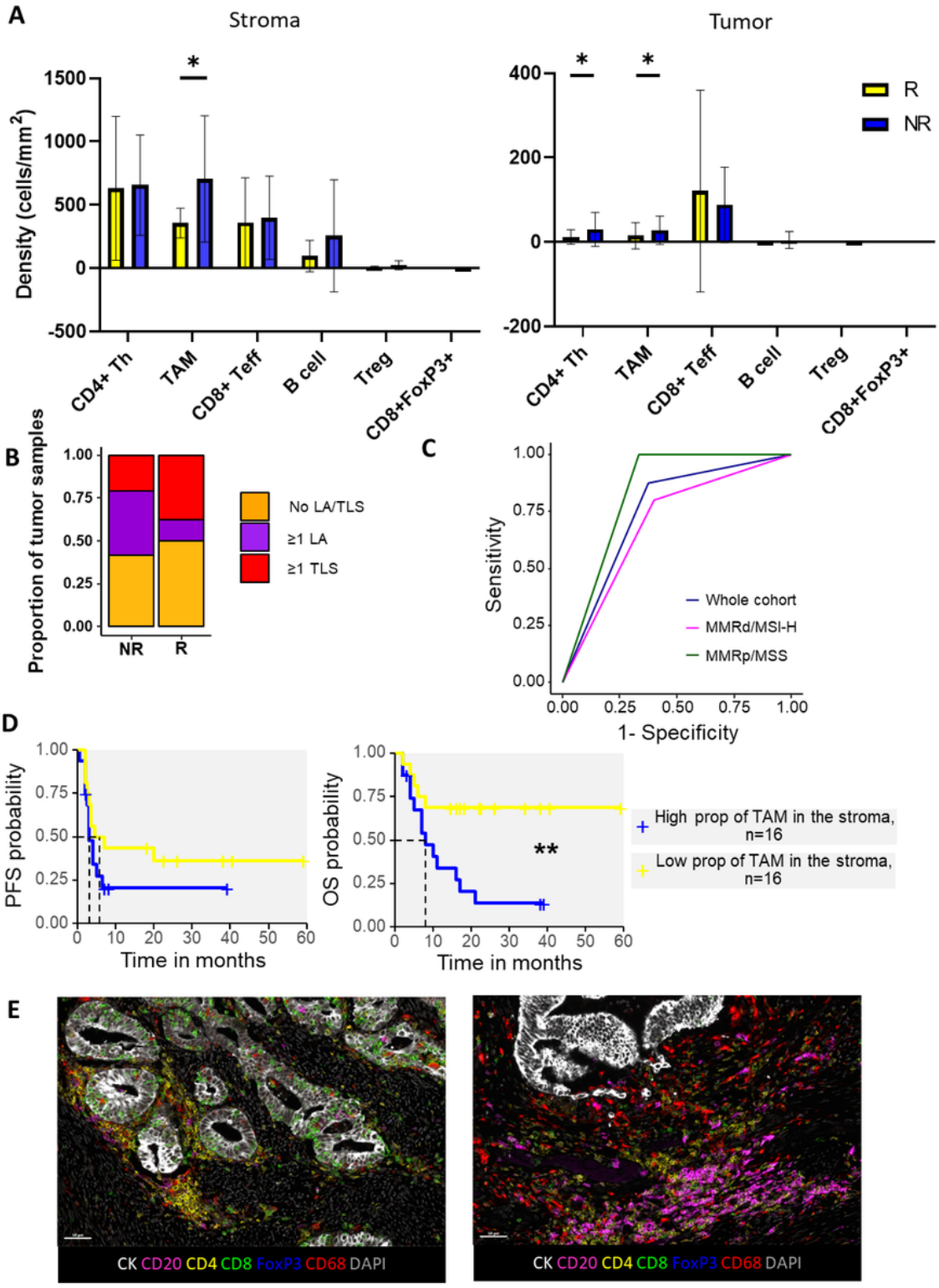

Figure 4

Resistance to immune checkpoint inhibitors is associated with a significant abundance of TAMs in the stroma in EC.

A – Number of cells/mm^2 (i.e., the density) of B cells, TAMs, $CD4^+$ T helper (Th) cells, $CD4^+$ regulatory T cells (Treg), $CD8^+$ effector T cells (Teff) and $CD8^+/FOXP3^+$ T cells both in the stroma (left) and within tumor islets (right) in responders (R) (yellow) and non-responders (NR) (blue). Mean and standard deviations are displayed.

B – Proportion of R (yellow) and NR (blue) samples with (≥1 lymphoid aggregate -LA- in the sample or ≥1 tertiary lymphoid structure -TLS- in the sample) and without TLS (no TLS in the sample). *P*-values < 0.05 were considered significant, with stars corresponding to * $p < 0.05$. If no stars are indicated, no statistically significant difference was found.

C – ROC curves representing the area under curve for the model considering a high/low proportion of TAMs in the stroma in the whole (blue), the MMRd/MSI-H (magenta) and MMRp/MSS (darkgreen) cohorts.

D – Survival curves representing the PFS (left) and OS (right) probability of patients presenting a low proportion of TAMs in the stroma (yellow) compared to others (blue).

E – Multiplex IF staining showing one NR EC patient with a high number of TAMs the stroma and a R patient with few TAMs in the stroma.

Supplementary Files

This is a list of supplementary files associated with this preprint. Click to download.

- SuppFigureandTable.docx